



# Phase-field simulations of crystal growth with adaptive mesh refinement

Yibao Li, Junseok Kim\*

Department of Mathematics, Korea University, Seoul 136-713, Republic of Korea

## ARTICLE INFO

### Article history:

Received 9 January 2012

Received in revised form 26 June 2012

Accepted 7 August 2012

Available online 4 September 2012

### Keywords:

Crystal growth

Phase-field simulation

Operator splitting

Multigrid method

Adaptive mesh refinement

## ABSTRACT

In this paper, we propose the phase-field simulation of dendritic crystal growth in both two- and three-dimensional spaces with adaptive mesh refinement, which was designed to solve nonlinear parabolic partial differential equations. The proposed numerical method, based on operator splitting techniques, can use large time step sizes and exhibits excellent stability. In addition, the resulting discrete system of equations is solved by a fast numerical method such as an adaptive multigrid method. Comparisons to uniform mesh method, explicit adaptive method, and previous numerical experiments for crystal growth simulations are presented to demonstrate the accuracy and robustness of the proposed method.

© 2012 Elsevier Ltd. All rights reserved.

## 1. Introduction

Crystal growth is a phase transformation from the liquid phase to the solid phase via heat transfer [1]. Predicting the shape of growing crystals is important for industrial crystallization processes [2]. Various numerical methods such as boundary integral [3–6], cellular automata [7–10], front-tracking [11–15], level-set [16–19], Monte-Carlo [20,21], and phase-field [22–42] have been developed to simulate crystal growth. Among these methods, the phase-field approach is widely used for modeling solidification problems since it avoids the explicit tracking of macroscopically sharp phase boundaries [29].

A great challenge in the simulation of crystal growth with various supercoolings is the large difference in time and length scales. The adaptive mesh refinement is faster and more efficient than a uniform mesh in simulating crystal growth because it allows concentration of effort and multi-resolution in space and time [27–41]. However most previous adaptive phase-field computations of dendrite crystal growth suffer from severe time step restrictions since they use explicit schemes [34–38]. Since the discrete Laplacian is used in the explicit scheme, its stability criterion becomes  $\Delta t \sim O(h^2)$ , where  $\Delta t$  is the time step and  $h$  is the mesh size. Thus the crystal growth simulation with various supercoolings is still very difficult.

To use large time steps, Rosam et al. [39,40] proposed a fully implicit, fully adaptive time and space discretization method for the

crystal growth simulation. Its stability is almost unconditionally stable although it is computationally more expensive than explicit ones per time step. To have better stability properties, a multiple time-step algorithm was presented in [41]. A larger time step is used for the flow-field calculations while reserving a finer time step for the phase-field evolution.

In our previous work [42], we introduced a fast, robust, and accurate operator splitting method for phase-field simulations of crystal growth with uniform mesh size, which allows large time steps, e.g.,  $\Delta t \sim O(h)$ . The main purpose of the present paper is to extend our previous work by incorporating adaptive mesh refinement. We will demonstrate stability, robustness, and accuracy of the proposed method by a set of representative numerical experiments.

This paper is organized as follows. In Section 2, we give the governing equations for crystal growth based on the phase-field model. In Section 3, computationally efficient operator splitting algorithm and adaptive mesh refinement are described. In Section 4, we present numerical results for solving the crystal growth simulation both in two and three dimensions. Finally, conclusions are given in Section 5.

## 2. The phase-field model

The basic equations of the phase-field model can be derived from a single Lyapounov functional [43]. We model the solidification in two and three dimensions using a standard form of phase-field equations. The model is given by

\* Corresponding author. Tel.: +82 2 3290 3077; fax: +82 2 929 8562.

E-mail addresses: [yibaoli@korea.ac.kr](mailto:yibaoli@korea.ac.kr) (Y. Li), [cfdkim@korea.ac.kr](mailto:cfdkim@korea.ac.kr) (J. Kim).

URL: <http://math.korea.ac.kr/~cfdkim/> (J. Kim).

$$\begin{aligned} \epsilon^2(\phi) \frac{\partial \phi}{\partial t} &= \nabla \cdot (\epsilon^2(\phi) \nabla \phi) + [\phi - \lambda U(1 - \phi^2)](1 - \phi^2) \\ &+ \left( |\nabla \phi|^2 \epsilon(\phi) \frac{\partial \epsilon(\phi)}{\partial \phi_x} \right)_x + \left( |\nabla \phi|^2 \epsilon(\phi) \frac{\partial \epsilon(\phi)}{\partial \phi_y} \right)_y \\ &+ \left( |\nabla \phi|^2 \epsilon(\phi) \frac{\partial \epsilon(\phi)}{\partial \phi_z} \right)_z, \end{aligned} \tag{1}$$

$$\frac{\partial U}{\partial t} = D \Delta U + \frac{1}{2} \frac{\partial \phi}{\partial t}, \tag{2}$$

where  $\phi \in [-1, 1]$  is the order parameter with  $\phi = 1$  in the solid phase and  $\phi = -1$  in the liquid phase.  $\phi = 0$  is defined as the interface of two phases.  $\epsilon(\phi)$  is the anisotropic function,  $\lambda$  is the dimensionless coupling parameter, and  $U = c_p(T - T_M)/L$  is the dimensionless temperature field. Here  $c_p$  is the specific heat at constant pressure,  $T_M$  is the melting temperature,  $L$  is the latent heat of fusion,  $D = \alpha \tau_0 / \epsilon_0^2$ ,  $\alpha$  is the thermal diffusivity,  $\tau_0$  is the characteristic time,  $\epsilon_0$  is the characteristic length.  $\lambda$  is given as  $\lambda = D/a_2$  with  $a_2 = 0.6267$  [28,29]. For the fourfold symmetry, anisotropic function  $\epsilon(\phi)$  with anisotropy strength  $\epsilon_4$ , is defined as:

$$\epsilon(\phi) = (1 - 3\epsilon_4) \left( 1 + \frac{4\epsilon_4}{1 - 3\epsilon_4} \frac{\phi_x^4 + \phi_y^4 + \phi_z^4}{|\nabla \phi|^4} \right).$$

### 3. Numerical solution

In this section, we propose a robust hybrid numerical method for the crystal growth simulation. For simplicity of exposition, we shall discretize Eqs. (1) and (2) in two-dimensional space, i.e.,  $\Omega = (a, b) \times (c, d)$ . Three-dimensional discretization is analogously defined. Let  $N_x$  and  $N_y$  be positive even integers,  $h = (b - a)/N_x$  be the uniform mesh size, and  $\Omega_h = \{(x_i, y_j) : x_i = (i - 0.5)h, y_j = (j - 0.5)h, 1 \leq i \leq N_x, 1 \leq j \leq N_y\}$  be the set of cell-centers. Let  $\phi_{ij}^n$  be approximations of  $\phi(x_i, y_j, n\Delta t)$ , where  $\Delta t = T/N_t$  is the time step,  $T$  is the final time, and  $N_t$  is the total number of time steps. Eqs. (1) and (2) are discretized in a similar manner as in [42]:

$$\begin{aligned} \epsilon^2(\phi^n) \frac{\phi^{n+1,1} - \phi^n}{\Delta t} &= 2\epsilon(\phi^n) \epsilon(\phi^n)_x \phi_x^n + 2\epsilon(\phi^n)_y \epsilon(\phi^n) \phi_y^n \\ &+ \left( \frac{16\epsilon(\phi^n) \epsilon_4 \phi_x (\phi_x^2 \phi_y^2 - \phi_y^4)}{|\nabla_d \phi|^4} \right)_x^n \\ &+ \left( \frac{16\epsilon(\phi^n) \epsilon_4 \phi_y (\phi_x^2 \phi_y^2 - \phi_x^4)}{|\nabla_d \phi|^4} \right)_y^n, \end{aligned} \tag{3}$$

$$\phi^{n+1,2} = \frac{\phi^{n+1,1}}{\sqrt{e^{-\frac{2\Delta t}{\epsilon^2(\phi^n)}} + (\phi^{n+1,1})^2 (1 - e^{-\frac{2\Delta t}{\epsilon^2(\phi^n)})}}}, \tag{4}$$

$$\epsilon^2(\phi^n) \frac{\phi^{n+1} - \phi^{n+1,2}}{\Delta t} = \epsilon^2(\phi^n) \Delta_d \phi^{n+1} - 4\lambda U^n F(\phi^{n+1,2}), \tag{5}$$

$$\frac{U^{n+1} - U^n}{\Delta t} = D \Delta_d U^{n+1} + \frac{\phi^{n+1} - \phi^n}{2\Delta t}, \tag{6}$$

where the discrete differentiation operator is  $\nabla_d \phi_{ij} = (\phi_{i+1,j} - \phi_{i-1,j}, \phi_{i,j+1} - \phi_{i,j-1})/(2h)$  and the discrete Laplacian operator is  $\Delta_d \phi_{ij} = (\phi_{i+1,j} + \phi_{i-1,j} - 4\phi_{ij} + \phi_{i,j+1} + \phi_{i,j-1})/h^2$ . With nine local points, we describe the following term

$$\left( \frac{\phi_x \epsilon(\phi) (\phi_x^2 \phi_y^2 - \phi_y^4)}{|\nabla_d \phi|^4} \right)_{x,ij} = \frac{\left( \frac{\phi_x \epsilon(\phi) (\phi_x^2 \phi_y^2 - \phi_y^4)}{|\nabla_d \phi|^4} \right)_{i+\frac{1}{2},j} - \left( \frac{\phi_x \epsilon(\phi) (\phi_x^2 \phi_y^2 - \phi_y^4)}{|\nabla_d \phi|^4} \right)_{i-\frac{1}{2},j}}{h},$$

where

$$\begin{aligned} &\left( \frac{\phi_x \epsilon(\phi) (\phi_x^2 \phi_y^2 - \phi_y^4)}{|\nabla_d \phi|^4} \right)_{i+\frac{1}{2},j}^n \\ &= \frac{(\epsilon(\phi_{i+1,j}^n) + \epsilon(\phi_{ij}^n)) (\phi_{i+1,j}^n - \phi_{ij}^n)^3 (\phi_{i+1,j+1}^n - \phi_{i+1,j-1}^n + \phi_{ij+1}^n - \phi_{ij-1}^n)^2}{h \left( (\phi_{i+1,j}^n - \phi_{ij}^n)^2 + (\phi_{i+1,j+1}^n - \phi_{i+1,j-1}^n + \phi_{ij+1}^n - \phi_{ij-1}^n)^2 / 4 \right)^2} + \delta \\ &= \frac{(\epsilon(\phi_{ij}^n) + \epsilon(\phi_{i-1,j}^n)) (\phi_{i-1,j}^n - \phi_{ij}^n)^3 (\phi_{i+1,j+1}^n - \phi_{i+1,j-1}^n + \phi_{ij+1}^n - \phi_{ij-1}^n)^4}{h \left( (\phi_{i+1,j}^n - \phi_{ij}^n)^2 + (\phi_{i+1,j+1}^n - \phi_{i+1,j-1}^n + \phi_{ij+1}^n - \phi_{ij-1}^n)^2 / 4 \right)^2} + \delta. \end{aligned}$$

The other terms can be described in a similar manner. Note that we added a small value  $\delta = 1e - 10$  in the denominator  $|\nabla_d \phi|^4$  to avoid singularities.

To solve the resulting system of discrete Eqs. (3)–(6) at the implicit time level, we use an adaptive mesh refinement [44,45], whose schematic diagram is shown in Fig. 1. In the adaptive approach, we introduce a hierarchy of increasingly finer grids,  $\Omega_{l+1}, \dots, \Omega_{l+r}$ , restricted to smaller and smaller subdomains, while the last hierarchy of global grids are  $\Omega_0, \Omega_1, \dots, \Omega_l$ . That is, we consider a hierarchy of grids,  $\Omega_0, \Omega_1, \dots, \Omega_{l+0}, \Omega_{l+1}, \dots, \Omega_{l+r}$ . Here we denote  $\Omega_{l+0}$  as level zero,  $\Omega_{l+1}$  as level one, and so on. For example, in Fig. 1,  $l^* = 3$ .

The grid is adapted dynamically based on the undivided gradient. First, we tag cells that contain the front, i.e., those in which the undivided gradient of the phase-field is greater than a critical value. Then, the tagged cells are grouped into rectangular patches by using a clustering algorithm as in Ref. [47]. These rectangular patches are refined to form the grids at the next level. The process is repeated until a specified maximum level is reached.

Next, we describe the adaptive full approximation storage cycle to solve the discrete system on the hierarchy of increasingly finer grids. First, let us rewrite Eqs. (5) and (6) as

$$N(\phi^{n+1}, U^{n+1}) = (\varphi^n, \psi^n),$$

where  $N(\phi^{n+1}, U^{n+1}) = \left( \frac{\phi^{n+1}}{\Delta t} - \Delta_d \phi^{n+1}, \frac{U^{n+1}}{\Delta t} - D \Delta_d U^{n+1} - \frac{\phi^{n+1}}{2\Delta t} \right)$  and the source term is  $(\varphi^n, \psi^n) = \left( \frac{\phi^{n+1,2}}{\Delta t} - \frac{4\lambda U^n F(\phi^{n+1,2})}{\epsilon^2(\phi^n)}, \frac{2U^n - \phi^n}{2\Delta t} \right)$ .

Using the above notations on all levels  $k = 0, 1, \dots, l, l + 1, \dots, l + l^*$ , an adaptive multigrid cycle is formally written as follows [46]:

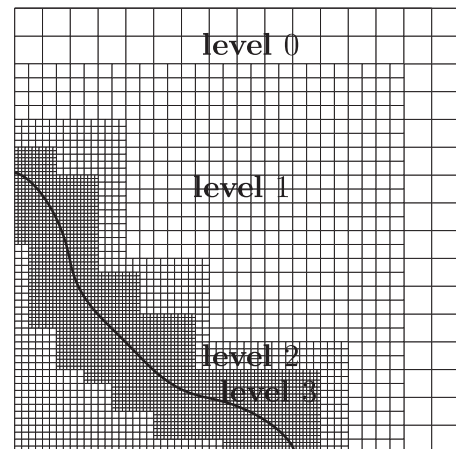


Fig. 1. Block-structured local refinement with four levels.

3.1. Adaptive cycle

We calculate  $\varphi_k^n, \psi_k^n$  on all levels and set the previous time solution as the initial guess, i.e.,  $(\varphi_k^0, U_k^0) = (\varphi_k^n, U_k^n)$ .

$$(\varphi_k^{m+1}, U_k^{m+1}) = \text{ADAPTIVEcycle}(k, \varphi_k^m, \varphi_{k-1}^m, U_k^m, U_{k-1}^m, N_k, \varphi_k^n, \psi_k^n, \nu).$$

(1) Presmoothing

- Compute  $(\bar{\varphi}_k^m, \bar{U}_k^m)$  by applying  $\nu$  smoothing steps to  $(\varphi_k^m, U_k^m)$  on  $\Omega_k$ .

$$(\bar{\varphi}_k^m, \bar{U}_k^m) = \text{SMOOTH}^\nu(\varphi_k^m, U_k^m, N_k, \varphi_k^n, \psi_k^n),$$

where one *SMOOTH* relaxation operator step consists of solving Eqs. (9) and (10) given below by a  $2 \times 2$  matrix inversion for each  $i$  and  $j$ . Rewriting Eqs. (5) and (6), we get

$$\left(\frac{1}{\Delta t} + \frac{4}{h^2}\right)\varphi_{ij}^{n+1} = \varphi_{ij}^n - \frac{\varphi_{i+1,j}^{n+1} + \varphi_{i-1,j}^{n+1} + \varphi_{i,j+1}^{n+1} + \varphi_{i,j-1}^{n+1}}{h^2}, \tag{7}$$

$$\left(\frac{1}{\Delta t} + \frac{4D}{h^2}\right)U_{ij}^{n+1} - \frac{\varphi_{ij}^{n+1}}{2\Delta t} = \psi_{ij}^n - \frac{D(U_{i+1,j}^{n+1} + U_{i-1,j}^{n+1} + U_{i,j+1}^{n+1} + U_{i,j-1}^{n+1})}{h^2}. \tag{8}$$

Next, we replace  $\varphi_{kl}^{n+1}$  and  $U_{kl}^{n+1}$  in Eqs. (7) and (8) with  $\bar{\varphi}_{kl}^m$  and  $\bar{U}_{kl}^m$  if  $k \leq i$  and  $l \leq j$ ; otherwise we replace them with  $\varphi_{kl}^m$  and  $U_{kl}^m$ , i.e.,

$$\left(\frac{1}{\Delta t} + \frac{4}{h^2}\right)\bar{\varphi}_{ij}^m = \varphi_{ij}^m - \frac{\varphi_{i+1,j}^m + \bar{\varphi}_{i-1,j}^m + \varphi_{i,j+1}^m + \bar{\varphi}_{i,j-1}^m}{h^2}, \tag{9}$$

$$\left(\frac{1}{\Delta t} + \frac{4D}{h^2}\right)\bar{U}_{ij}^m - \frac{\bar{\varphi}_{ij}^m}{2\Delta t} = \psi_{ij}^m - \frac{D(U_{i+1,j}^m + \bar{U}_{i-1,j}^m + U_{i,j+1}^m + \bar{U}_{i,j-1}^m)}{h^2}. \tag{10}$$

(2) Coarse-grid correction

- Compute

$$(\hat{\varphi}_{k-1}^m, \hat{U}_{k-1}^m) = \begin{cases} I_k^{k-1}(\bar{\varphi}_k^m, \bar{U}_k^m) & \text{on } \Omega_{k-1} \cap \Omega_k, \\ (\varphi_{k-1}^m, U_{k-1}^m) & \text{on } \Omega_{k-1} - \Omega_k. \end{cases}$$

- Compute the coarse grid source term

$$(\varphi_{k-1}^n, \psi_{k-1}^n) = \begin{cases} I_k^{k-1}\{(\varphi_k^n, \psi_k^n) - N_k(\bar{\varphi}_k^m, \bar{U}_k^m)\}, \\ + N_{k-1}I_k^{k-1}(\bar{\varphi}_k^m, \bar{U}_k^m) & \text{on } \Omega_{k-1} \cap \Omega_k, \\ (\varphi_{k-1}^n, \psi_{k-1}^n) & \text{on } \Omega_{k-1} - \Omega_k. \end{cases}$$

- Compute an approximate solution  $(\hat{\varphi}_{k-1}^m, \hat{U}_{k-1}^m)$  of the coarse grid equation on  $\Omega_{k-1}$ , i.e.,

$$N_{k-1}(\hat{\varphi}_{k-1}^m, \hat{U}_{k-1}^m) = (\varphi_{k-1}^n, \psi_{k-1}^n). \tag{11}$$

If  $k = 1$ , we explicitly invert a  $2 \times 2$  matrix to obtain the solution. If  $k > 1$ , we solve Eq. (11) by using  $(\bar{\varphi}_{k-1}^m, \bar{U}_{k-1}^m)$  as an initial approximation to perform an adaptive multigrid  $k$ -grid cycle:

$$(\hat{\varphi}_{k-1}^m, \hat{U}_{k-1}^m) = \text{ADAPTIVEcycle}(k-1, \bar{\varphi}_{k-1}^m, \varphi_{k-2}^m, \bar{U}_{k-1}^m, U_{k-2}^m, N_{k-1}, \varphi_{k-1}^n, \psi_{k-1}^n, \nu).$$

- Compute the correction at  $\Omega_{k-1} \cap \Omega_k$ .  $(\hat{u}_{k-1}^m, \hat{v}_{k-1}^m) = (\hat{\varphi}_{k-1}^m, \hat{U}_{k-1}^m) - (\bar{\varphi}_{k-1}^m, \bar{U}_{k-1}^m)$ .

- Set the solution at the other points of  $\Omega_{k-1} - \Omega_k$ .

$$(\varphi_{k-1}^{m+1}, U_{k-1}^{m+1}) = (\hat{\varphi}_{k-1}^m, \hat{U}_{k-1}^m).$$

- Interpolate the correction to  $\Omega_k$ .  $(\hat{u}_k^m, \hat{v}_k^m) = I_{k-1}^k(\hat{u}_{k-1}^m, \hat{v}_{k-1}^m)$ .

- Compute the corrected approximation on  $\Omega_k$ .

$$(\varphi_k^m \text{ after CGC}, U_k^m \text{ after CGC}) = (\bar{\varphi}_k^m + \hat{u}_k^m, \bar{U}_k^m + \hat{v}_k^m).$$

(3) Postsmoothing

$$(\varphi_k^{m+1}, U_k^{m+1}) = \text{SMOOTH}^\nu(\varphi_k^m \text{ after CGC}, U_k^m \text{ after CGC}, N_k, \varphi_k^n, \psi_k^n).$$

This completes the description of an adaptive multigrid cycle. For additional details about the adaptive multigrid cycle, please refer to [46].

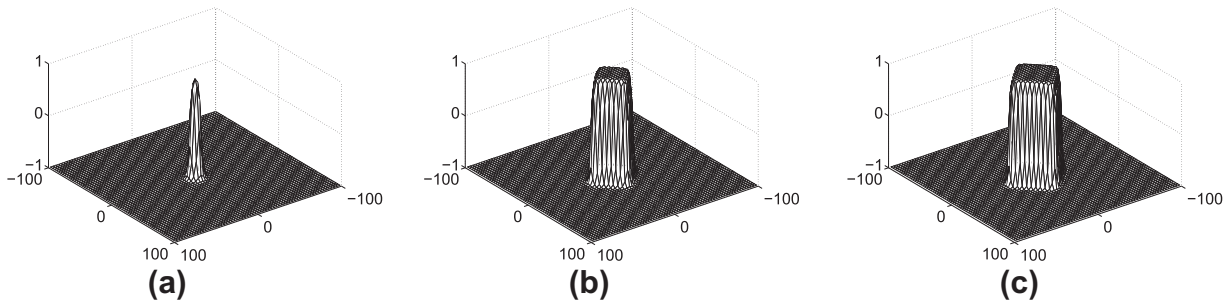


Fig. 2. The stability of crystal growth with different time steps: (a)  $\Delta t = 2.24$  ( $256 \times 256$  mesh), (b)  $\Delta t = 1.17$  ( $512 \times 512$  mesh), and (c)  $\Delta t = 0.59$  ( $1024 \times 1024$  mesh).

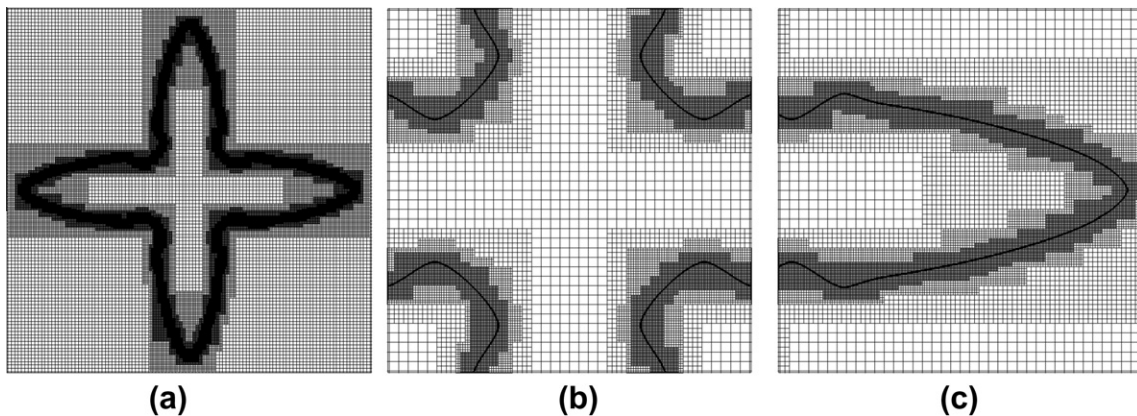


Fig. 3. A sample adaptive mesh in different views in two dimensions. (a) whole view, (b) and (c) closeup views.

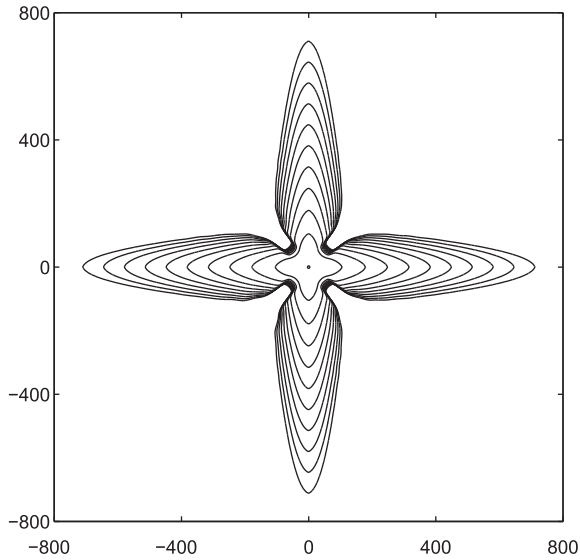


Fig. 4. The evolution for crystal growth in two dimensions.

4. Numerical results

In this section, we perform numerical experiments for two- and three-dimensional solidification to validate that our proposed scheme is accurate, efficient, and robust. For two-dimensional tests, unless otherwise specified, we take the initial state as

$$\phi(x, y, 0) = \tanh\left(\frac{R_0 - \sqrt{x^2 + y^2}}{\sqrt{2}}\right),$$

$$U(x, y, 0) = \frac{\Delta(1 - \phi(x, y, 0))}{2} \approx \begin{cases} 0 & \text{if } \phi > 0 \\ \Delta & \text{else.} \end{cases}$$

The zero level set ( $\phi = 0$ ) represents a circle of radius  $R_0$ . From the dimensionless variable definition, the value  $U = 0$  corresponds to the melting temperature of the pure material, while  $U = \Delta$  is the initial undercooling. The capillary length  $d_0$  is defined as  $d_0 = a_1/\lambda$  [39,43], where  $a_1 = 0.8839$  and  $\lambda = 3.1913$  [39]. And the other parameters are chosen as  $\epsilon_4 = 0.05$  and  $D = 2$ .

4.1. Stability of our proposed algorithm

As mentioned in Section 1, explicit schemes [34–38] suffer from time step restrictions  $\Delta t \leq O(h^2)$  for the stability. In order to overcome the restriction of time step, Li et al. [42] proposed a fast, robust, and accurate operator splitting method for phase-field simulations of crystal growth. The authors showed that their method can use large time step sizes  $\Delta t \sim O(h)$ . Here, we consider a set of increasingly finer grids to show the stability of our proposed method. The computational domain is  $\Omega = (-100, 100)^2$  with  $2^n \times 2^n$  mesh grids for  $n = 8, 9,$  and  $10$ . The numerical solutions are computed up to  $T = 128.91$ , with time steps  $\Delta t = 3h$ . Other parameters are  $R_0 = 14d_0$  and  $\Delta = -0.55$ . Fig. 2 shows crystal shape at time  $T = 128.91$  with different time steps. From these results, we can observe that our proposed method also allows large time step sizes.

4.2. Evolution for crystal growth in two- and three-dimensional spaces

In this experiment, we will show the evolution of crystal growth in two and three dimensions with adaptive mesh method. A sample two dimensional adaptive meshes with different views are shown in Fig. 3.

The computational domains are set as  $\Omega = (-800, 800)^2$  with  $l^* = 4$  levels in two dimensions and  $\Omega = (-200, 200)^3$  with  $l^* = 4$  levels in three dimensional case. And other parameters are chosen as  $\Delta t = 0.4, R_0 = 14d_0,$  and  $\Delta = -0.55$ . The calculations are run up to time  $T = 8000$  in two dimensions and  $T = 480$  in three dimensions.

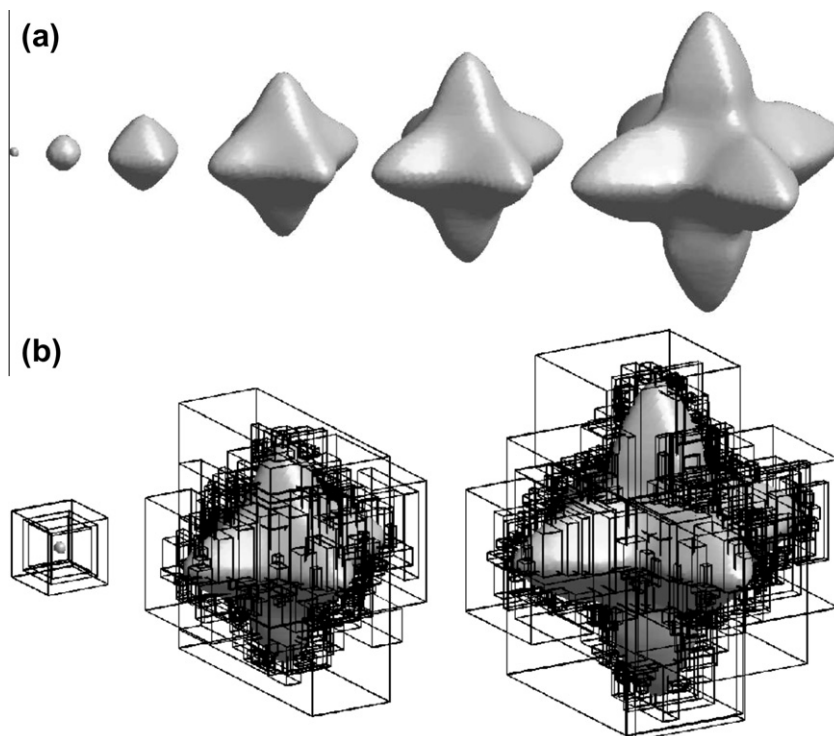


Fig. 5. Snapshots of three-dimensional evolution of crystal growth. (a) crystal shape at times  $t = 0, 20, 40, 160, 240,$  and  $480$  (from left to right). (b) The bounding boxes at times  $t = 0, 240,$  and  $480$ .

**Table 1**

Comparison of CPU time and tip positions calculated by the explicit scheme and our proposed scheme.

Method	Time step	Tip position	CPU time (h)
Explicit method	0.01	45.94	0.10
Proposed method	0.01	45.91	0.60
Proposed method	0.20	44.48	0.02

Fig. 4 shows the temporal evolution of crystal interface. Fig. 5(a) shows three-dimensional structures at times  $t = 0, 20, 40, 160, 240$ , and 480 (from left to right). And in Fig 5(b), we show the bounding boxes at times  $t = 0, 240$ , and 480 to show the structured local refinement.

#### 4.3. Comparison between our proposed method and explicit adaptive method

In general, an explicit scheme is fast, however, the overall CPU time for long time integration larger than an implicit scheme, which can use larger time steps. This is true for the adaptive method used here. In order to show our proposed method is more efficient than explicit adaptive methods, we consider CPU time comparison test in two dimensions. The computational domain is set as  $\Omega = (-200, 200)^2$  with  $l^* = 3$  levels. The minimum element size  $h_{min} = 0.39$ ,  $R_0 = 15d_0$ , and  $\Delta = -0.55$  are used. Since the explicit adaptive method suffers the time step size limitation, here we use a time step  $\Delta t = 0.01$ . For our proposed method, we use time step  $\Delta t = 0.01$  and  $\Delta t = 0.2$ . The calculations are run up to time

$T = 200$ . We list the tip position of crystal and CPU time in Table 1. From these results, we can observe that our proposed method with  $\Delta t = 0.01$  needs more CPU time than the explicit method. However, with  $\Delta t = 0.2$  our proposed method is about 5 times faster than the explicit method. Tip positions with different methods are similar.

#### 4.4. Comparison with uniform mesh simulation

In this experiment, we will compare the results obtained on uniform meshes and on adaptively refined meshes for two and three dimensions to show the efficiency and accuracy of our proposed method. For two dimensions, the computational domain is set as  $\Omega = (-400, 400)^2$  with  $1024 \times 1024$  mesh grids for uniform mesh calculation and  $l^* = 3$  levels for the adaptive mesh method. And in three dimensions, we use  $\Omega = (-100, 100)^3$ ,  $256 \times 256 \times 256$ , and  $l^* = 3$ . With time step  $\Delta t = 0.3$ , the calculations are run up to time  $T = 1800$  and  $T = 240$  in two and three dimensions, respectively. The comparisons with uniform meshes and adaptively refined meshes in two and three dimensions are drawn in the first row and in the second row of Fig. 6, respectively. As can be observed, the agreement between the results computed by uniform meshes and adaptive meshes is good. In the two-dimensional calculation, the taken CPU times are 16.15 h and 0.82 h for uniform and adaptive meshes, respectively. In the three-dimensional calculation, the taken CPU times are 29.15 h and 2.71 h for uniform and adaptive meshes, respectively.

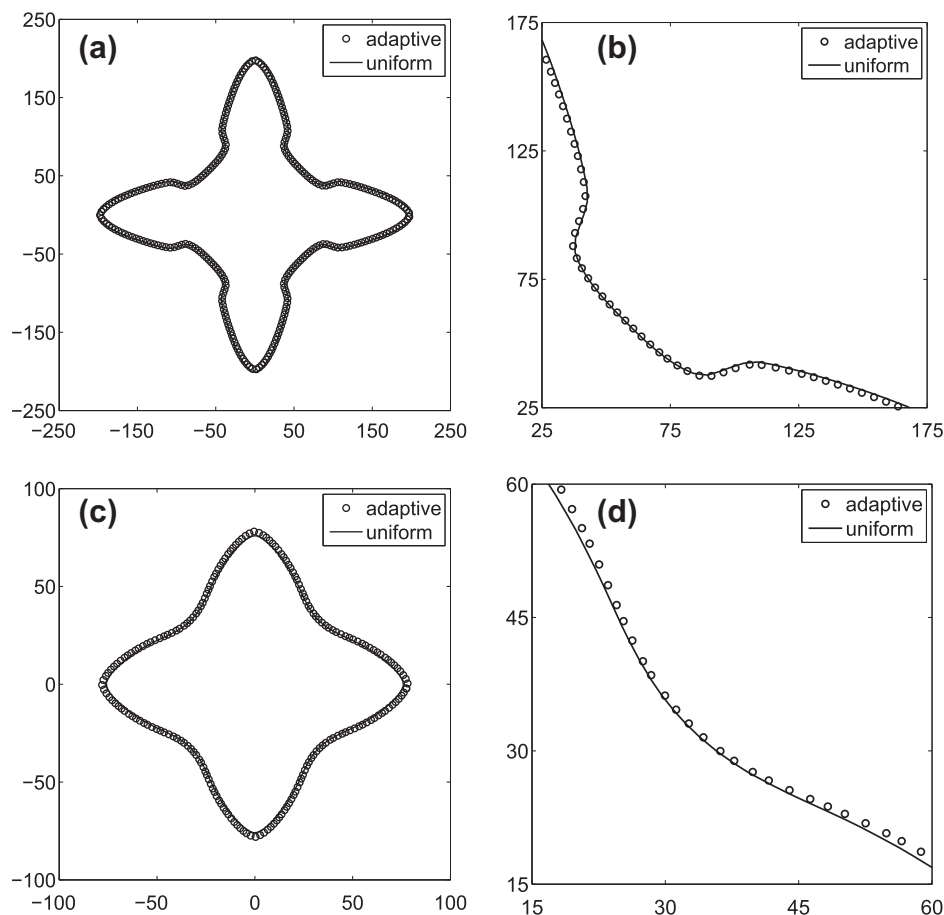


**Fig. 6.** The comparison between uniform meshes and adaptive meshes in two and three dimensions. First and second rows are two and three dimensional cases, respectively. (a) crystal shape at  $t = 1800$ . (c)  $y$ - $z$  plane of crystal shape at  $t = 240$ . (b) and (d) are closeup views of (a) and (c), respectively.

**Table 2**

Comparison of dimensionless steady-state tip velocities calculated by the proposed scheme ( $V_{tip} = Vd_0/D$ ), the results in [42] ( $V_{tip}^{LLK}$ ), results in [29] ( $V_{tip}^{KR}$ ), and Green's function calculations ( $V_{tip}^{GF}$ ).

$\Delta$	$\epsilon_4$	$D$	$d_0/W_0$	$V_{tip}^{LLK}$	$V_{tip}^{KR}$	$V_{tip}^{GF}$	$V_{tip}$
-0.55	0.05	2	0.277	0.01710	0.01680	0.01700	0.01700
-0.55	0.05	3	0.185	0.01740	0.01750	0.01700	0.01720
-0.55	0.05	4	0.139	0.01720	0.01740	0.01700	0.01710
-0.50	0.05	3	0.185	0.01030	0.01005	0.00985	0.00997
-0.45	0.05	3	0.185	0.00599	0.00557	0.00545	0.00537

**4.5. Comparison of the dimensionless steady-state tip velocities**

To demonstrate the accuracy of our proposed method, we compare the dimensionless steady-state tip velocities obtained by our proposed adaptive method with the results in [29,42] and Green's function calculations [29]. This test is performed on the domain  $\Omega = (-200,200)^2$  with  $l^* = 3$ , the minimum element size  $h_{min} = 0.39$ ,  $\Delta t = 0.15$ ,  $R_0 = 3.462$ ,  $W_0 = 1$ , and  $\lambda = D/a_2$ .

To calculate the steady-state velocity, we use a quadratic polynomial approximation. We only describe the procedure along the y-axis since the crystal is symmetric. Given three points,  $(x_{k-1}, y_{k-1})$ ,  $(x_k, y_k)$ , and  $(x_{k+1}, y_{k+1})$  on the interface, where  $y_k$  is a maximum value. Let the quadratic polynomial approximation passing these three points be  $y = \alpha x^2 + \beta x + \gamma$ . Then we can find the tip position  $y_*$  which satisfies the following conditions:  $y'(x_*) = 0$  and  $y_* = \alpha x_*^2 + \beta x_* + \gamma$ .

The crystal tip velocity is defined as the finite difference of tip positions from consecutive time steps. From a set of numerical results in Table 2, we can observe that values obtained by our proposed scheme are in good agreement with results of previous methods over the whole range of  $\Delta$ ,  $\epsilon_4$ ,  $D$ , and  $d_0/W_0$  investigated here.

**4.6. Dendritic growth at low undercooling**

For low undercoolings, it requires much longer time to reach a steady-state tip velocity due to the lower growth rate. Furthermore an extremely large domain should be used to avoid the far field boundary effect. In this case, the adaptive mesh refinement method is a better choice to overcome it. Here, we consider low undercoolings such as  $\Delta = -0.25$  and  $\Delta = -0.1$ . The computational domain is  $\Omega = (-6400,6400)^2$  with the base mesh grids,  $32 \times 32$ .  $l^* = 9$  is used and the minimum grid spacing  $h_{min}$  is 0.78. With time step  $\Delta t = 0.4$ , the numerical solutions for  $\Delta = -0.25$  and  $\Delta = -0.1$  are computed up to  $T = 4000$  and  $T = 40000$ , respectively. Other parameters are  $d_0 = 0.403$ ,  $R_0 = 100d_0$ ,  $D = 13$ , and  $\lambda = 20.744$ . Fig. 7 shows the evolution of tip velocity ( $V_{tip}$ ) for  $\Delta = -0.25$  and  $\Delta = -0.1$  with our proposed method, the results in [32], and solvability theory [49,50]. The numerical results show good agreement with previous results.

Next, we consider steady-state tip velocities in three dimensions. There is the simple relationship which was obtained by Ivantsov [50]:

$$\Delta = -Pe \exp(Pe) \int_{Pe}^{\infty} \frac{\exp(-s)}{s} ds,$$

where  $Pe = R_{tip}V_{tip}/(2D)$  is the Peclet number and  $R_{tip}$  is the tip radius. The stability constant  $\sigma = 2Dd_0/(R_{tip}^2V_{tip})$  was used in [49,50]. Here we choose  $\sigma = 0.02$ . Thus for given  $\Delta$ ,  $D$ , and  $d_0$ , we can compute  $V_{tip}$ . In numerical experiment, we perform the simulation on the domain  $\Omega = (-100,100) \times (-100,100) \times (0,800)$  with the base mesh grids,  $8 \times 8 \times 32$ . Here  $l^* = 5$  and the minimum grid spacing  $h_{min} = 0.78$  are used. The other parameters are same as those used in two-dimensional space except for  $R_0 = 50d_0$ .

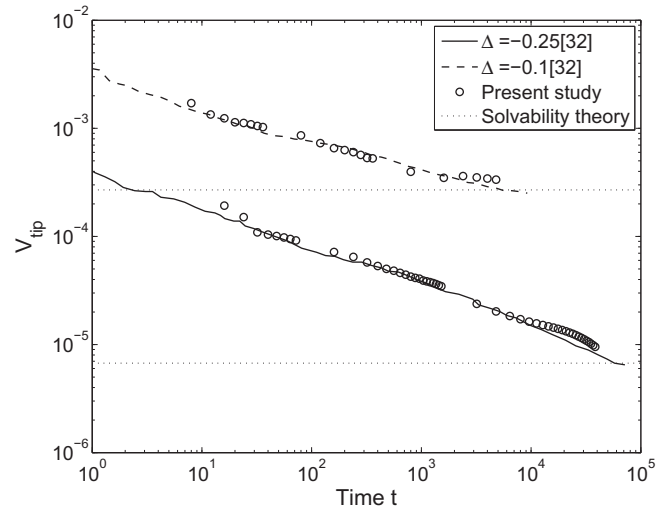


**Fig. 7.** Evolution of tip velocity at  $\Delta = -0.25$  and  $\Delta = -0.1$ . In order to compare the results in [32] and the results computed by solvability theory, we put them together.

**Table 3**

Comparison of dimensionless steady-state tip velocities calculated by our proposed method and the analytic solution.

Case	$\Delta = -0.25$	$\Delta = -0.1$
Analytic solution	0.00251	0.000139
Numerical solution	0.00252	0.000148

Comparisons with theoretical solutions are drawn in Table 3. From these results, we can observe that dimensionless steady-state tip velocities obtained by our proposed scheme are in good agreement with the analytic solutions at low undercoolings.

**5. Conclusion**

In this paper, we have proposed the phase-field simulation of dendritic crystal growth in both two- and three-dimensional spaces with adaptive mesh refinement, which was designed to solve nonlinear parabolic partial differential equations. The proposed operator splitting numerical method can use large time step sizes and exhibits excellent stability. The resulting discrete system of equations is solved by an adaptive multigrid method. Comparisons to uniform mesh method, explicit adaptive method, and previous numerical experiments for crystal growth simulations were presented to demonstrate the accuracy and robustness of the proposed method. In numerical experiments, the stability of the method was found as  $\Delta t \leq 3h$ . Compared to uniform mesh method and explicit adaptive method, our method achieved the equivalent accuracy with less computational cost. A set of computations for the dimensionless steady-state tip velocity showed a good agreement with results published in [29,42]. In particular, for low undercoolings, a good agreement with previous study [32] and analytic solution [48–50] was found as well. These simulations confirm that our proposed method is efficient and accurate.

**Acknowledgments**

This research was supported by Basic Science Research Program through the National Research Foundation of Korea (NRF) funded by the Ministry of Education, Science and Technology (No. 2011-0023794). The authors also wish to thank the anonymous referee

for the constructive and helpful comments on the revision of this article.

## References

- [1] S. Li, J. Lowengrub, P. Leo, V. Cristini, Nonlinear theory of self-similar crystal growth and melting, *J. Cryst. Growth* 267 (2004) 703–713.
- [2] X.Y. Liu, E.S. Boek, W.J. Briels, P. Bennema, Prediction of crystal growth morphology based on structural analysis of the solid–fluid interface, *Nature* 374 (1995) 342–345.
- [3] S. Li, J.S. Lowengrub, P.H. Leo, Nonlinear morphological control of growing crystals, *Phys. D* 208 (2005) 209–219.
- [4] D.I. Meiron, Boundary integral formulation of the two-dimensional symmetric model of dendritic growth, *Phys. D* 23 (1986) 329–339.
- [5] J.A. Sethian, J. Strain, Crystal growth and dendritic solidification, *J. Comput. Phys.* 98 (1992) 231–253.
- [6] J. Strain, A boundary integral approach to unstable solidification, *J. Comput. Phys.* 85 (1989) 342–389.
- [7] D. Li, R. Li, P. Zhang, A cellular automaton technique for modelling of a binary dendritic growth with convection, *Appl. Math. Model.* 31 (2007) 971–982.
- [8] H. Yin, S.D. Felicelli, A cellular automaton model for dendrite growth in magnesium alloy AZ91, *Model. Simulat. Mater. Sci. Eng.* 17 (2009) 075011.
- [9] M.F. Zhu, C.P. Hong, A modified cellular automaton model for the simulation of dendritic growth in solidification of alloys, *ISIJ Int.* 41 (2001) 436–445.
- [10] M.F. Zhu, S.Y. Lee, C.P. Hong, Modified cellular automaton model for the prediction of dendritic growth with melt convection, *Phys. Rev. E* 69 (2004) 061610.
- [11] N. Al-Rawahi, G. Tryggvason, Numerical simulation of dendritic solidification with convection: two-dimensional geometry, *J. Comput. Phys.* 180 (2002) 471–496.
- [12] T. Ihle, Competition between kinetic and surface tension anisotropy in dendritic growth, *Eur. Phys. J. B* 16 (2000) 337–344.
- [13] D. Juric, G. Tryggvason, A front-tracking method for dendritic solidification, *J. Comput. Phys.* 123 (1996) 127–148.
- [14] G. Tryggvason, B. Bunner, A. Esmaeeli, D. Juric, N. Al-Rawahi, W. Tauber, J. Han, S. Nas, Y.-J. Jan, A front-tracking method for the computations of multiphase flow, *J. Comput. Phys.* 169 (2001) 708–759.
- [15] P. Zhao, J.C. Heinrich, D.R. Poirier, Fixed mesh front-tracking methodology for finite element simulations, *Int. J. Numer. Methods Eng.* 61 (2004) 928–948.
- [16] S. Chen, B. Merriman, S. Osher, P. Smereka, A simple level set method for solving Stefan problem, *J. Comput. Phys.* 135 (1997) 8–29.
- [17] F. Gibou, R. Fedkiw, R. Caflisch, S. Osher, A level set approach for the numerical simulation of dendritic growth, *J. Sci. Comput.* 19 (2002) 183–199.
- [18] Y.-T. Kim, N. Goldenfeld, J. Dantzig, Computation of dendritic microstructures using a level set method, *Phys. Rev. E* 62 (2000) 2471–2474.
- [19] K. Wang, A. Chang, L.V. Kale, J.A. Dantzig, Parallelization of a level set method for simulating dendritic growth, *J. Parallel Distrib. Comput.* 66 (2006) 1379–1386.
- [20] M. Plapp, A. Karma, Multiscale finite-difference-diffusion-Monte-Carlo method for simulating dendritic solidification, *J. Comput. Phys.* 165 (2000) 592–619.
- [21] T.P. Schulze, Simulation of dendritic growth into an undercooled melt using kinetic Monte Carlo techniques, *Phys. Rev. E* 78 (2008) 020601.
- [22] J.-M. Debierre, A. Karma, F. Celestini, R. Guérin, Phase-field approach for faceted solidification, *Phys. Rev. E* 68 (2003) 041604.
- [23] R. Kobayashi, Modeling and numerical simulations of dendritic crystal growth, *Phys. D* 63 (1993) 410–423.
- [24] S.-L. Wang, R.F. Sekerka, Algorithms for phase field computation of the dendritic operating state at large supercoolings, *J. Comput. Phys.* 127 (1996) 110–117.
- [25] J.A. Warren, W.J. Boettinger, Prediction of dendritic growth and microsegregation patterns in a binary alloy using the phase-field method, *Acta Metall. Mater.* 43 (1995) 689–703.
- [26] Y. Xu, J.M. McDonough, K.A. Tagavi, A numerical procedure for solving 2D phase-field model problems, *J. Comput. Phys.* 218 (2006) 770–793.
- [27] A. Karma, Y.H. Lee, M. Plapp, Three-dimensional dendrite-tip morphology at low undercooling, *Phys. Rev. E* 61 (2000) 3996–4006.
- [28] A. Karma, W.-J. Rappel, Phase-field method for computationally efficient modeling of solidification with arbitrary interface kinetics, *Phys. Rev. E* 53 (1996) 3017–3020.
- [29] A. Karma, W.-J. Rappel, Quantitative phase-field modeling of dendritic growth in two and three dimensions, *Phys. Rev. E* 57 (1998) 4323–4349.
- [30] C.C. Chen, C.W. Lan, Efficient adaptive three-dimensional phase-field simulation of dendritic crystal growth from various supercoolings using rescaling, *J. Cryst. Growth* 311 (2009) 702–706.
- [31] C.C. Chen, Y.L. Tsai, C.W. Lan, Adaptive phase field simulation of dendritic crystal growth in a forced flow: 2D vs. 3D morphologies, *Int. J. Heat Mass Transfer* 52 (2009) 1158–1166.
- [32] C.W. Lan, C.M. Hsu, C.C. Liu, Y.C. Chang, Adaptive phase field simulation of dendritic growth in a forced flow at various supercoolings, *Phys. Rev. E* 65 (2002) 061601.
- [33] C.J. Shih, M.H. Lee, C.W. Lan, A simple approach toward quantitative phase field simulation for dilute-alloy solidification, *J. Cryst. Growth* 282 (2005) 515–524.
- [34] J.-H. Jeong, N. Goldenfeld, J.A. Dantzig, Phase field model for three-dimensional dendritic growth with fluid flow, *Phys. Rev. E* 64 (2001) 041602.
- [35] B. Nestler, D. Danilov, P. Galenko, Crystal growth of pure substances: phase-field simulations in comparison with analytical and experimental results, *J. Comput. Phys.* 207 (2005) 221–239.
- [36] N. Provatas, N. Goldenfeld, J. Dantzig, Efficient computation of dendritic microstructures using adaptive mesh refinement, *Phys. Rev. Lett.* 80 (1998) 3308–3311.
- [37] N. Provatas, N. Goldenfeld, J. Dantzig, Adaptive mesh refinement computation of solidification microstructures using dynamic data structures, *J. Comput. Phys.* 148 (1999) 265–290.
- [38] J.C. Ramirez, C. Beckermann, A. Karma, H.-J. Diepers, Phase-field modeling of binary alloy solidification with coupled heat and solute diffusion, *Phys. Rev. E* 69 (2004) 051607.
- [39] J. Rosam, P.K. Jimack, A. Mullis, A fully implicit, fully adaptive time and space discretisation method for phase-field simulation of binary alloy solidification, *J. Comput. Phys.* 225 (2007) 1271–1287.
- [40] J. Rosam, P.K. Jimack, A. Mullis, An adaptive, fully implicit multigrid phase-field model for the quantitative simulation of non-isothermal binary alloy solidification, *Acta Mater.* 56 (2008) 4559–4569.
- [41] X. Tong, C. Beckermann, A. Karma, Q. Li, Phase-field simulations of dendritic crystal growth in a forced flow, *Phys. Rev. E* 63 (2001) 061601.
- [42] Y. Li, H.G. Lee, J. Kim, A fast, robust, and accurate operator splitting method for phase-field simulations of crystal growth, *J. Cryst. Growth* 321 (2011) 176–182.
- [43] J.S. Langer, in: *Directions in Condensed Matter*, World Scientific, Singapore, 1986, pp. 164–186.
- [44] A.S. Almgren, J.B. Bell, P. Colella, L.H. Howell, M.L. Welcome, A conservative adaptive projection method for the variable density incompressible Navier–Stokes equations, *J. Comput. Phys.* 142 (1998) 1–46.
- [45] M. Sussman, A.S. Almgren, J.B. Bell, P. Colella, L.H. Howell, M.L. Welcome, An adaptive level set approach for incompressible two-phase flows, *J. Comput. Phys.* 148 (1999) 81–124.
- [46] U. Trottenberg, C. Oosterlee, A. Schüller, *Multigrid*, Academic Press, USA, 2001.
- [47] M.J. Berger, I. Rigoutsos, Technical Report NYU-501, New York University-CIMS, 1991.
- [48] D. Kessler, J. Koplik, H. Levine, Pattern selection in fingered growth phenomena, *Adv. Phys.* 37 (1988) 255–339.
- [49] J.S. Langer, Instabilities and pattern formation in crystal growth, *Rev. Mod. Phys.* 52 (1980) 1–28.
- [50] G.P. Ivantsov, Temperature field around spherical cylindrical and needleshaped crystals which grow in supercooled melt, *Dokl. Akad. Nauk SSSR* 58 (1947) 567–569.